Journal of
Synchrotron Radiation
ISSN 0909-0495
Editors: **G. Ice, Å. Kvick and T. Ohta**

Reconstruction of magnetization density in two-dimensional samples from soft X-ray speckle patterns using the multiple-wavelength anomalous diffraction method

T. O. Menteş, C. Sánchez-Hanke and C. C. Kao

J. Synchrotron Rad. (2002). **9**, 90–95

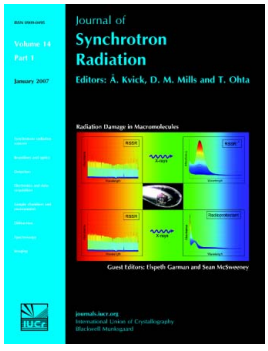

Reconstruction of magnetization density in two-dimensional samples from soft X-ray speckle patterns using the multiple-wavelength anomalous diffraction method

T. O. Menteş,* C. Sánchez-Hanke and C. C. Kao

NSLS, Brookhaven National Laboratory, Upton, NY 11973, USA. E-mail: tmentes@bnl.gov

A non-destructive technique for imaging magnetic domains in thin films and two-dimensional magnetic structures using coherent soft X-ray scattering and the multiple-wavelength anomalous diffraction method (MAD) is proposed. The method exploits the strong energy dependence in the magnetic scattering amplitude for $3d$ transition metals near the $L_{2,3}$ absorption edges and $4f$ elements near the $M_{4,5}$ absorption edges. The phase information required in the reconstruction algorithm is derived from the interference between the charge and magnetic scattering amplitudes. Magnetic speckle patterns from the magnetic domain distribution in an artificially defined Fe thin film are used to demonstrate this reconstruction algorithm. Circularly and linearly polarized incident light are examined separately to investigate the effect of polarization on the capability of the method.

Keywords: reconstruction; magnetization density; speckle; phase problem.

1. Introduction

The solution of the phase problem in the structure determination of crystals using multiple-wavelength anomalous diffraction (MAD) is well established (Karle, 1994; Hendrickson, 1991). The general idea is based on the strong wavelength dependence of the anomalous scattering amplitudes. By measuring the intensity at different wavelengths around a resonance, one can obtain linearly independent equations, which can be used to solve the structure factors of the crystal. This method is similar to the 'multiple isomorphous replacement' approach, where the structure factors are changed by replacing one type of scatterer by another type, instead of changing the energy around a resonance (Hendrickson, 1991).

MAD uses the fact that the phase information for the structure factors are in the interference terms between different types of scatterers. However, using incoherent light limits the applicability of the method to crystals. The idea of reconstructing the charge density of non-periodic objects, using coherent incident light and oversampling the intensities, was suggested by Sayre (1952, 1980), and has recently been realised experimentally (Miao *et al.*, 1999). The method is based on the fact that, under certain constraints, overdetermination of the Fourier amplitudes of the charge density is sufficient to find the phases uniquely.

In the case of imaging a magnetic sample, the same problem of missing phases arises. To find the non-periodic magnetic structure, which is in general different from the charge density, one may think that in principle the same method of oversampling the speckle pattern can be used. However, scattering of photons by a magnetic moment is purely a relativistic effect, and therefore is much smaller compared with charge scattering. Away from any resonance, the total scattering amplitude is given by Blume (1985),

$$f = f_{\rm D} r_0 \left\{ Z\left(\hat{\boldsymbol{\epsilon}}_f^* \cdot \hat{\boldsymbol{\epsilon}}_0\right) - i\left(\hbar\omega/mc^2\right)\left[\tfrac{1}{2}\vec{\mathbf{L}}(\vec{\mathbf{K}}) \cdot \vec{\mathbf{A}} + \vec{\mathbf{S}}(\vec{\mathbf{K}}) \cdot \vec{\mathbf{B}}\right]\right\}, \quad (1)$$

where $f_{\rm D}$ is the Debye–Waller factor, r_0 is the electron radius, $\hat{\boldsymbol{\epsilon}}$ is the polarization unit vector, $\vec{\mathbf{L}}$ and $\vec{\mathbf{S}}$ are orbital and spin densities, $\vec{\mathbf{K}}$ is the momentum transfer, $\vec{\mathbf{k}}_0 - \vec{\mathbf{k}}_f$, and $\vec{\mathbf{A}}$ and $\vec{\mathbf{B}}$ are polarization-dependent factors. As seen in (1), the magnetic part, which is the second term on the right-hand side, is suppressed by a factor $\hbar\omega/mc^2$ compared with the charge scattering term.

When ω is close to a resonance, that is an electric multipole transition between core and valence levels, a large enhancement in the sensitivity to the magnetization is observed in certain elements (Gibbs *et al.*, 1988). The contribution to the resonant exchange scattering from the electric $2L$-pole transition in a magnetic ion is given by Hannon *et al.* (1988),

$$f_{EL}\left(\hat{\boldsymbol{\epsilon}}_0, \hat{\mathbf{k}}_0, \hat{\boldsymbol{\epsilon}}_f^*, \hat{\mathbf{k}}_f\right) = 2\lambda f_{\rm D} \sum_{M=-L}^{L} \left[\hat{\boldsymbol{\epsilon}}_f^* \cdot \mathbf{Y}_{LM}^{(e)}\left(\hat{\mathbf{k}}_f\right) \mathbf{Y}_{LM}^{*(e)}\left(\hat{\mathbf{k}}_0\right) \cdot \hat{\boldsymbol{\epsilon}}_0\right] F_{LM}^{(e)}(\omega). \quad (2)$$

In the case of dipole transitions only, the total scattering amplitude is

$$\begin{aligned} f^{(\rm total)} = {} & \left(\hat{\boldsymbol{\epsilon}}_f^* \cdot \hat{\boldsymbol{\epsilon}}_0\right)\left\{(3/8\pi)\lambda\left[F_{11}^{(e)} + F_{1-1}^{(e)}\right] - r_e Z\right\} \\ & + (3/8\pi)\lambda\left\{i\left(\hat{\boldsymbol{\epsilon}}_f^* \times \hat{\boldsymbol{\epsilon}}_0\right) \cdot \hat{\mathbf{z}}_J\left[F_{1-1}^{(e)} - F_{11}^{(e)}\right]\right. \\ & \left. + \left(\hat{\boldsymbol{\epsilon}}_f^* \cdot \hat{\mathbf{z}}_J\right)\left(\hat{\boldsymbol{\epsilon}}_0 \cdot \hat{\mathbf{z}}_J\right)\left[2F_{10}^{(e)} - F_{11}^{(e)} - F_{1-1}^{(e)}\right]\right\}, \end{aligned} \quad (3)$$

where $\hat{\mathbf{z}}_J$ is the unit vector pointing in the direction of the local moment of the ion and F_{LM} are the transition matrix elements, which can be obtained experimentally from the measured absorption coefficient $[F_{11}^{(e)} + F_{1-1}^{(e)}]$, the magnetic circular dichroism (MCD) $[F_{11}^{(e)} - F_{1-1}^{(e)}]$, and the magnetic linear dichroism $[2F_{10}^{(e)} - F_{11}^{(e)} - F_{1-1}^{(e)}]$. Therefore, the total scattering amplitude can be rewritten in terms of the charge and magnetic parts of the forward scattering amplitude,

$$f_i = \left(\hat{\boldsymbol{\epsilon}}_f^* \cdot \hat{\boldsymbol{\epsilon}}_0\right)\left(f'_{\rm chg} + if''_{\rm chg}\right) - i\left(\hat{\boldsymbol{\epsilon}}_f^* \times \hat{\boldsymbol{\epsilon}}_0\right) \cdot \hat{\mathbf{m}}_i\left(f'_{\rm mag} + if''_{\rm mag}\right), \quad (4)$$

where $f'_{\rm chg,mag}$ and $f''_{\rm chg,mag}$ are determined from MCD and photoabsorption measurements. Fig. 1 shows these factors for Fe in units of electron radius (Chen *et al.*, 1995). Note that only the out-of-plane component of magnetization $\hat{\mathbf{m}}$ is considered in the following simulation; therefore, the second-order term in $\hat{\mathbf{m}}$ has dropped out.

From inspection of (3), it is clear that the missing phase information of the Fourier transform of the magnetization can in principle be found using the interference between charge and magnetic scattering amplitudes of the magnetic ion. The proposed method is similar to MAD, except interference between different types of scatterers is used in MAD. Here, this idea will be demonstrated using small-angle scattering with coherent soft X-rays.

2. Simulation

The simulated sample is a two-dimensional thin film of Fe or Fe alloys. The film thickness is chosen such that the easy axis for magnetization is normal to the plane. The illuminated sample size is of the order of a few micrometres. Magnetization is assumed to be uniform along the film thickness, as well as in domains of size much larger than the nearest-neighbour interatomic spacing.

The incident light is assumed to be a plane wave with the wavevector parallel to the sample normal. The scattered intensity is simulated as observed on a CCD detector several centimetres away from the sample in the transmission geometry (Fig. 2).

Within the Born approximation, the scattering cross section is related to the Fourier transform of the scattering amplitude by

$$\frac{d\sigma(\vec{\mathbf{K}})}{d\Omega} = \left| \sum_i f_i^{\sigma} \exp(i\vec{\mathbf{K}} \cdot \vec{\mathbf{r}}_i) \right|^2 + \left| \sum_i f_i^{\pi} \exp(i\vec{\mathbf{K}} \cdot \vec{\mathbf{r}}_i) \right|^2, \quad (5)$$

where the σ and π components correspond to the polarization states perpendicular and parallel to the scattering plane defined by $(\hat{\mathbf{k}}_0, \hat{\mathbf{k}}_f)$ and $\vec{\mathbf{K}}$ is the momentum transfer, $\vec{\mathbf{k}}_0 - \vec{\mathbf{k}}_f$. f_i is the scattering amplitude for the scatterer i, which can be represented as in (3). The photon flux observed in a solid angle $\Delta\Omega$ is given by

$$I(\vec{\mathbf{K}}) = \frac{I_0}{A_{\rm tot}} \frac{d\sigma(\vec{\mathbf{K}})}{d\Omega} \Delta\Omega, \quad (6)$$

where I_0 is the incident flux in photons per second and $A_{\rm tot}$ is the total illuminated area on the sample.

The charge distribution is taken as uniform on the scale set by the wavelength (~ 2 nm), and the sample is divided into domains of equal size. The size of the domains is much smaller than the illuminated area on the sample, but larger than 2 nm. These domains are defined such that the magnetization is uniform within the domain boundaries. Hence the summation in (5) runs over effective domains rather than single scatterers, where the scattering from a single domain is modelled by convoluting the scattering amplitude with the form factor corresponding to the size and the shape of the domain. In the case of rectangular domains which have dimensions t_x and t_y in the sample plane (transverse plane), this form factor is

$$F(\vec{\mathbf{K}}) = N \frac{\sin(K_x t_x/2)\sin(K_y t_y/2)}{(K_x t_x/2)(K_y t_y/2)}, \quad (7)$$

where N is the total number of scatterers in the domain.

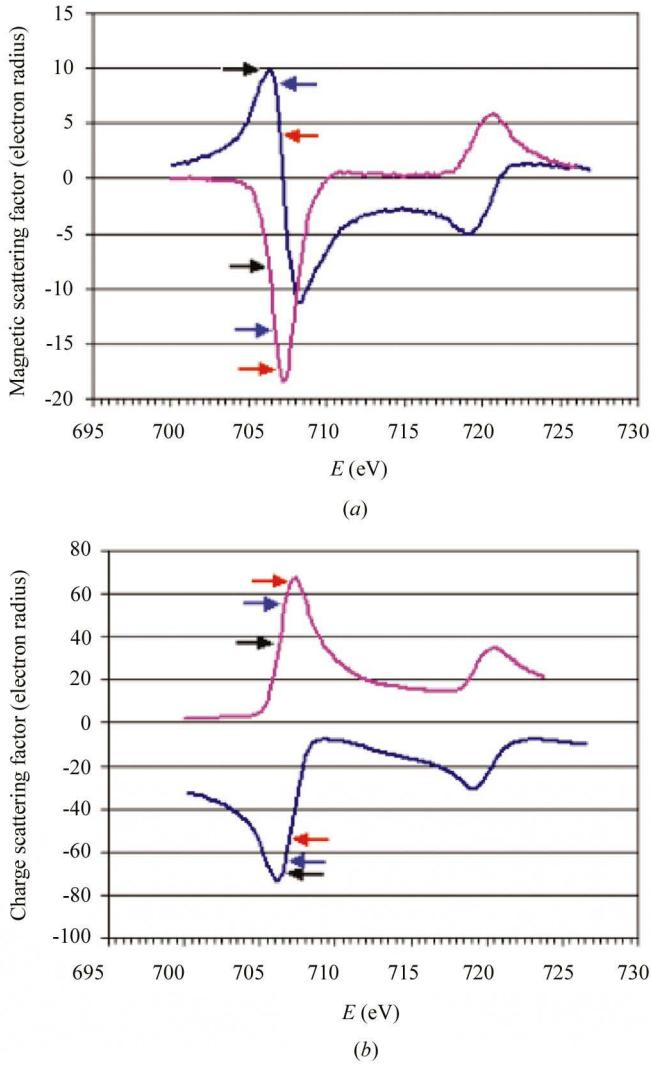

Figure 1
Fe magnetic scattering factor (*a*) and charge scattering factor (*b*) obtained from MCD and absorption measurements (Chen *et al.*, 1995). The arrows point to the energies used in the reconstruction, as described in §3. Blue curve: real; pink curve: imaginary.

3. Reconstruction

As seen in (5) and (6) in the previous section, the observed intensity on the detector is proportional to the square of the Fourier transform of the scattering amplitude. In order to reconstruct the magnetization density, we need to recover the missing phases of the Fourier components of the magnetization. The method used is based on the fact that the atomic scattering factors have very strong wavelength dependence around specific resonances.

This reconstruction technique can be described as follows. First, the observed intensity can be written in the following form,

$$\begin{aligned} I(\vec{\mathbf{K}}) &\propto |F_1 + F_2 M(\vec{\mathbf{K}})|^2 \\ &\propto |F_1|^2 + |F_2|^2 |M(\vec{\mathbf{K}})|^2 + F_1^* F_2 M(\vec{\mathbf{K}}) + F_1 F_2^* M^*(\vec{\mathbf{K}}), \end{aligned} \quad (8)$$

where F_1 and F_2 are complex coefficients depending on the charge density, polarization, momentum transfer and wavelength, and $M(\vec{\mathbf{K}})$ is the Fourier transform of the magnetization. F_1 and F_2 can be calculated for a given charge density with known atomic scattering factors and scattering geometry. Also, the charge density of the sample can be determined independently from off-resonant speckle pattern as demonstrated by Miao *et al.* (1999).† Consequently, the only unknowns are the real and imaginary parts of $M(\vec{\mathbf{K}})$. Obviously it is not possible to solve for both with only one equation. However, if the λ dependence of $M(\vec{\mathbf{K}})$ for small shifts in the incident energy of

† Note that the method which we describe in this paper relies on the information on charge density in order to find the magnetization. In cases where this information is missing, one might think that the problem of having more unknowns, the phase and the amplitude of the charge structure factor, can be overcome by obtaining more independent equations in the form of (8), rather than using other methods. However, this idea does not work as the interference terms between charge and magnetic scattering, written explicitly in (11), contain only the difference of the phases of charge and magnetic structure factors. Therefore, they cannot be solved separately. In other words, the phase information from the charge density is needed to be able to find the magnetization.

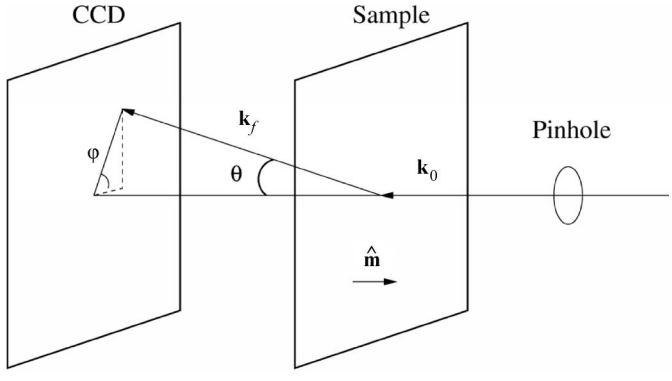

Figure 2
Scattering geometry.

the order of an electronvolt can be ignored, then, by using the strong dependence of F_1 and F_2 on the wavelength, more than one independent equation for $M(\vec{\mathbf{K}})$ and $M^*(\vec{\mathbf{K}})$ can be obtained simply by tuning the energy around the resonance.

Since the phase information is derived from the interference terms in (8), a complication may arise for thin-film samples due to the fact that F_1, which is the resonant and non-resonant charge-scattering contribution, drops very quickly with increasing momentum transfer for a uniform charge distribution. This makes the last two terms in (8) very small, thus limiting the $\vec{\mathbf{K}}$ range that can be used in the reconstruction. The phase information is lost when the dependence of $M(\vec{\mathbf{K}})$ on λ for a given pixel becomes comparable with the interference terms. This dependence can in principle be reduced by adjusting the sample-to-CCD distance such that it is inversely proportional to the wavelength. Owing to the fact that the drop in the charge scattering as a function of the momentum transfer is limited by the finite sample size, the uniformity of the charge density sets a limit on the sample size that can be imaged for a given resolution.

3.1. Linear polarization

Consider the case where the incident polarization is linear. For simplicity, the beam direction is chosen parallel to the z axis and the electric field vector along the y axis. If we represent the scattered beam direction as (θ, φ) in polar coordinates, then σ and π polarization unit vectors are as follows,

$$\begin{aligned}\hat{\boldsymbol{\epsilon}}_\sigma &= (\sin\varphi, -\cos\varphi, 0),\\ \hat{\boldsymbol{\epsilon}}_\pi &= (\cos\theta\cos\varphi, \cos\theta\sin\varphi, -\sin\varphi).\end{aligned} \tag{9}$$

Therefore, the scattering amplitude for a single scatterer becomes

$$\begin{aligned}f_i^{\,\sigma} &= -\cos\varphi\,(f'_{\rm chg} + if''_{\rm chg})\rho_i - i\sin\varphi\, m_i(f'_{\rm mag} + if''_{\rm mag}),\\ f_i^{\,\pi} &= \cos\theta\sin\varphi\,(f'_{\rm chg} + if''_{\rm chg})\rho_i - i\cos\theta\cos\varphi\, m_i(f'_{\rm mag} + if''_{\rm mag}),\end{aligned} \tag{10}$$

in units of electron radius. ρ_i and m_i are the charge and magnetization of the ith scatterer, respectively. If we take these amplitudes and substitute them into (5) and (6), we obtain for the intensity,

$$\begin{aligned}I(\vec{\mathbf{K}}, \lambda) = {} & A(\vec{\mathbf{K}}, \lambda)|F_c(\vec{\mathbf{K}})|^2 + B(\vec{\mathbf{K}}, \lambda)|M(\vec{\mathbf{K}})|^2\\ & + C(\vec{\mathbf{K}}, \lambda)|F_c(\vec{\mathbf{K}})||M(\vec{\mathbf{K}})|\cos(\varphi_c - \varphi)\\ & + D(\vec{\mathbf{K}}, \lambda)|F_c(\vec{\mathbf{K}})||M(\vec{\mathbf{K}})|\sin(\varphi_c - \varphi),\end{aligned} \tag{11}$$

where M and F_c are the Fourier transforms of the magnetization and charge densities, respectively, and A, B, C and D are coefficients which depend on the direction and strongly on the wavelength. These coefficients can be obtained from the experimentally determined scattering amplitudes. Normalizing out the constant parts and keeping only the direction and wavelength-dependent factors,

$$\begin{aligned}A(\vec{\mathbf{K}}, \lambda) &= (1 - \sin^2\theta\sin^2\varphi)\,|f_{\rm chg}|^2,\\ B(\vec{\mathbf{K}}, \lambda) &= (1 - \sin^2\theta\cos^2\varphi)\,|f_{\rm mag}|^2,\\ C(\vec{\mathbf{K}}, \lambda) &= 2\sin^2\theta\sin\varphi\cos\varphi\,|f_{\rm chg}||f_{\rm mag}|\sin(\varphi_{\rm chg} - \varphi_{\rm mag}),\\ D(\vec{\mathbf{K}}, \lambda) &= 2\sin^2\theta\sin\varphi\cos\varphi\,|f_{\rm chg}||f_{\rm mag}|\cos(\varphi_{\rm chg} - \varphi_{\rm mag}),\\ f'_{\rm chg,mag} + f''_{\rm chg,mag} &= |f_{\rm chg,mag}|\exp(\varphi_{\rm chg,mag}).\end{aligned} \tag{12}$$

Further, the Fourier transforms, M and F_c, can be written down as follows,

$$\begin{aligned}M(\vec{\mathbf{K}}) &= |M|\exp(\varphi) = \sum_i m_i \exp(i\vec{\mathbf{K}}\cdot\vec{\mathbf{r}}_i)F(\vec{\mathbf{K}}),\\ F_c(\vec{\mathbf{K}}) &= |F_c|\exp(\varphi_c) = \textstyle\sum_i \rho_i \exp(i\vec{\mathbf{K}}\cdot\vec{\mathbf{r}}_i)F(\vec{\mathbf{K}}),\end{aligned} \tag{13}$$

where the summation runs over the domains, and $F(\vec{\mathbf{K}})$ is the form factor corresponding to the domain size and shape. m_i is the out-of-plane magnetization component in domain i, and takes values from -1 to $+1$. As the magnetization is real, we have the following relation for its Fourier transform,

$$M^*(-\vec{\mathbf{K}}) = M(\vec{\mathbf{K}}). \tag{14}$$

Noting the $\vec{\mathbf{K}}$ dependence of the coefficients, and using the realness of the magnetization as in (14), we obtain another equation in M,

$$\begin{aligned}I(-\vec{\mathbf{K}}, \lambda) = {} & A(\vec{\mathbf{K}}, \lambda)|F_c(\vec{\mathbf{K}})|^2 + B(\vec{\mathbf{K}}, \lambda)|M(\vec{\mathbf{K}})|^2\\ & + C(\vec{\mathbf{K}}, \lambda)|F_c(\vec{\mathbf{K}})||M(\vec{\mathbf{K}})|\cos(\varphi_c - \varphi)\\ & - D(\vec{\mathbf{K}}, \lambda)|F_c(\vec{\mathbf{K}})||M(\vec{\mathbf{K}})|\sin(\varphi_c - \varphi).\end{aligned} \tag{15}$$

From (11), $M(\vec{\mathbf{K}})$ cannot be uniquely identified, but it can be restricted to lie on a circle in the complex plane. A shift in the energy around the resonance of a few electronvolts will change the coefficients A, B, C, D, and the intensity I, hence giving an independent equation for $M(\vec{\mathbf{K}})$. The solution for the transform of the magnetization is one of the two complex values obtained from these second-order equations. Therefore, in principle, intensity measurements at two different wavelengths, with the additional constraint from (15), is capable of giving a unique solution for the phase of the 'magnetic structure factor'. However, as we mentioned earlier, the coefficients C and D in the interference terms are very small owing to the uniformity of the charge distribution and a $\sin^2\theta$ factor from the polarization dependence, and the two circles lie very close to each other. In essence, this severely limits the $\vec{\mathbf{K}}$ range that can be used in the reconstruction. In this case, we have to supplement this method with other techniques such as oversampling. However, linear polarization can be used effectively to image in-plane magnetization in reflection geometry.

3.2. Circular polarization

In the case of circular polarization, keeping the same reference frame with the beam direction parallel to the z axis, the incident circular polarization unit vectors in rectangular coordinates are given by

$$\begin{aligned}\hat{\boldsymbol{\epsilon}}_0^{\,(+)} &= 1/2^{1/2}(1, i, 0),\\ \hat{\boldsymbol{\epsilon}}_0^{\,(-)} &= 1/2^{1/2}(1, -i, 0).\end{aligned} \tag{16}$$

As in the case of linear polarization, ignoring the constant factors, the coefficients A, B, C and D depend on $\vec{\mathbf{K}}$ and λ, and are given by

$$\begin{aligned}A(\vec{\mathbf{K}}, \lambda) &= \tfrac{1}{2}(1 + \cos^2\theta)|f_{\rm chg}|^2,\\ B(\vec{\mathbf{K}}, \lambda) &= \tfrac{1}{2}(1 + \cos^2\theta)|f_{\rm mag}|^2,\\ C(\vec{\mathbf{K}}, \lambda) &= \pm(1 + \cos^2\theta)|f_{\rm chg}||f_{\rm mag}|\sin(\varphi_{\rm chg} - \varphi_{\rm mag}),\\ D(\vec{\mathbf{K}}, \lambda) &= \pm(1 + \cos^2\theta)|f_{\rm chg}||f_{\rm mag}|\cos(\varphi_{\rm chg} - \varphi_{\rm mag}),\end{aligned} \tag{17}$$

where the upper sign in the expressions for C and D is for left circular polarization and the lower sign is for right circular polarization. Comparing (17) with (12), we see that the contribution of the last two terms of (11) to the intensity is suppressed by a factor of $\sin^2\theta$ for the linear polarized incident light relative to the circular polarization case.

In the following, a 5×5 μm square magnetic sample with out-of-plane domain pattern is shown in Fig. 3. The thickness of the sample is 10 monolayers, and is implicitly included in the normalization constant of the form factor. Coherent incident flux is taken to be 10^8 photons s^{-1}, an assumption based on the undulator source for the

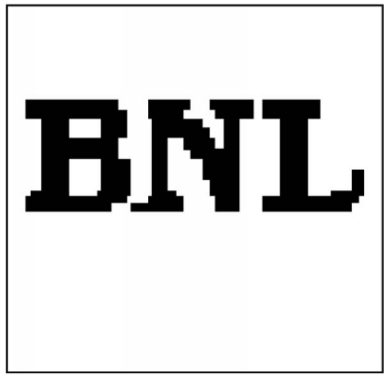

Figure 3
Simulated thin-film sample domain pattern. White and black areas correspond to up-spin and down-spin domains, respectively.

X1B beamline at the NSLS. In the simulations, the sample-to-CCD distance is 15 cm, and the CCD consists of a 256 × 256 array of 24 μm pixels. For a sample thickness of 10 monolayers, about 10^4 scattered photons s^{-1} are recorded on the detector. Also included is a constant factor to account for the exposure time and the photon to electron–hole pair conversion in the CCD.

The simulated diffraction images on the CCD detector for left circular incident polarization at three energies (706.3 eV, 706.7 eV and 707.0 eV) around the L_{III} edge of Fe are given in Fig. 4. It is possible to see the differences in the speckle patterns due to the magnetic contrast. The reconstruction of the magnetization using these three wavelengths is given in Fig. 5. As mentioned earlier, in principle two images are sufficient to obtain a unique solution for the Fourier transform of the magnetization, with the addition of the realness constraint. The third image is used to replace this additional information. The reason for this is that the realness condition, as seen in (14), requires identification of the pixel corresponding to $-\vec{\mathbf{K}}$, given $\vec{\mathbf{K}}$. However, the definition of the conjugate wavevector involves the centre of the diffraction pattern, which carries an error of the order of the speckle size in the actual experiment, because of the missing data due to the beamstop. Hence, we try to avoid the use of (14) as a means of finding solutions for the transform of the magnetization.

Note that in Fig. 5 the reconstructed magnetization varies from −1 to +1. The largest errors are about 15%, with a width of 5%. The error is due to the fact that a flat CCD is used, and that it has pixels of finite size. This problem can in principle be avoided by using a spherical pixel detector.

3.3. Beamstop

As the intensity becomes very high in the centre of the diffraction pattern, a beamstop is necessary to protect the CCD from radiation damage. Hence, the information within approximately 1 mrad of the origin of the reciprocal space is lost. The effect of this loss is demonstrated in Fig. 6, where the beamstop is taken to be a 5 × 5 square pixel. As can be roughly observed comparing the original 'BNL' image with Fig. 6, setting the Fourier transform to zero at the centre tends to wipe out the broadest features in the reconstructed image, such as the total magnetization. This can be observed in the histogram given on the right-hand side, which shows that both peaks shift to the left in order to decrease this total magnetization.

A possible method for recovering the lost information would be to use a modified version of the oversampling technique. In this way, one would use the method described in this paper for all points in the momentum space except for the centre region blocked by the beamstop, and obtain both the phases and the amplitudes in this region of the diffraction pattern by an iterative algorithm, which uses finite illuminated sample size as an additional constraint.

The beamstop may not be a significant problem depending on the sample that is being examined. To demonstrate this, we have taken the domain structure of a $GdFe_2$ film from Peters *et al.* (2000). The left-hand panel in Fig. 7 is a magnetic force microscope image of the stripe domains. The centre panel is the simulated speckle pattern, and the right-hand panel shows the reconstructed magnetization density for a 10 × 10 pixel beamstop. In this case, the magnetization is more uniform compared with the 'BNL' sample, and most of the information in the diffraction pattern is concentrated on a circle that corresponds to the ∼110 nm average domain spacing. Therefore, having a beamstop in the centre does not cause as much loss of information as in the 'BNL' case.

4. Conclusion

A technique for magnetic imaging, analogous to the multiple wavelength anomalous diffraction method used in crystallography, has been proposed. The phase information required in the reconstruction process is provided by the interference between the charge and magnetic scattering amplitudes of the scatter. Consequently, knowledge of charge density is necessary for the reconstruction of magnetization density. The proposed reconstruction algorithm was successfully tested using an artificially defined magnetic domain pattern. The effect of polarization and missing information due to the beamstop are also studied. As expected from the polarization dependence of the magnetic scattering amplitude, circular polariza-

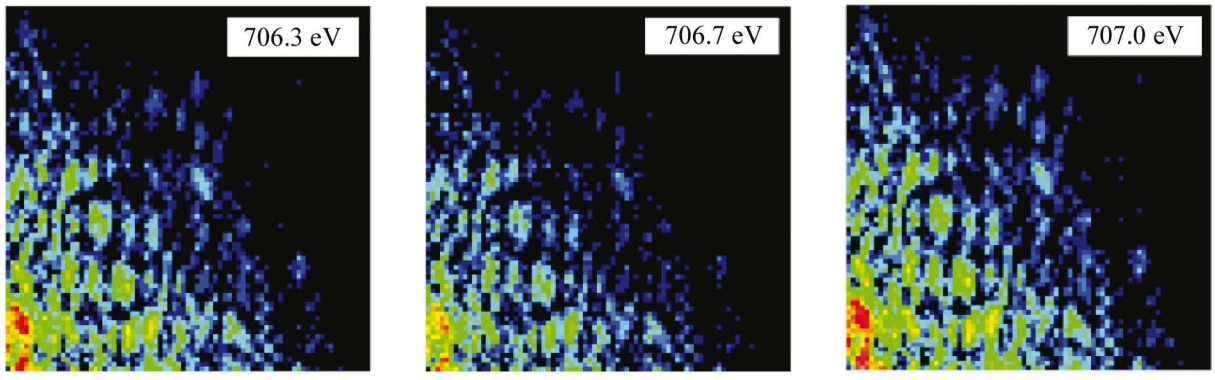

Figure 4
Simulated speckle patterns at three different energies. The incident beam has left circular polarization. The intensities are shown on a logarithm scale.

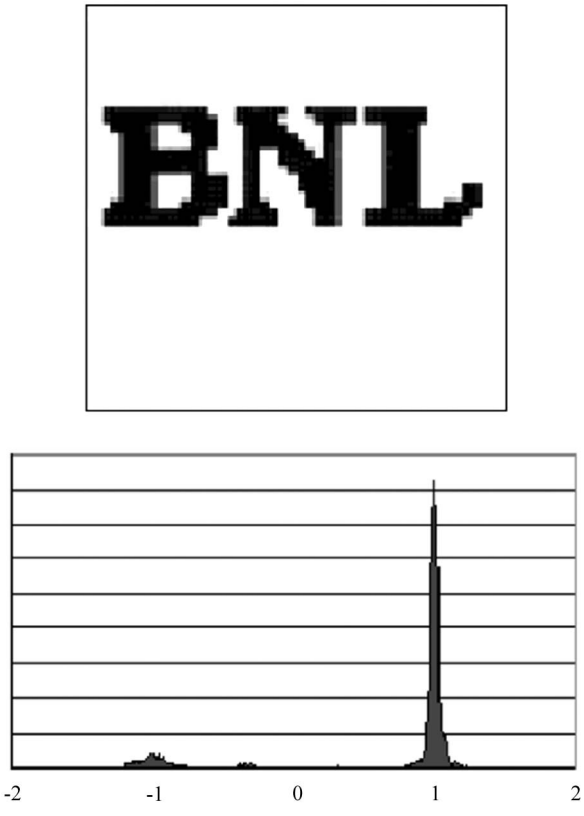

Figure 5
Reconstructed magnetization density. The histogram underneath shows the distribution of reconstructed magnetization for each domain.

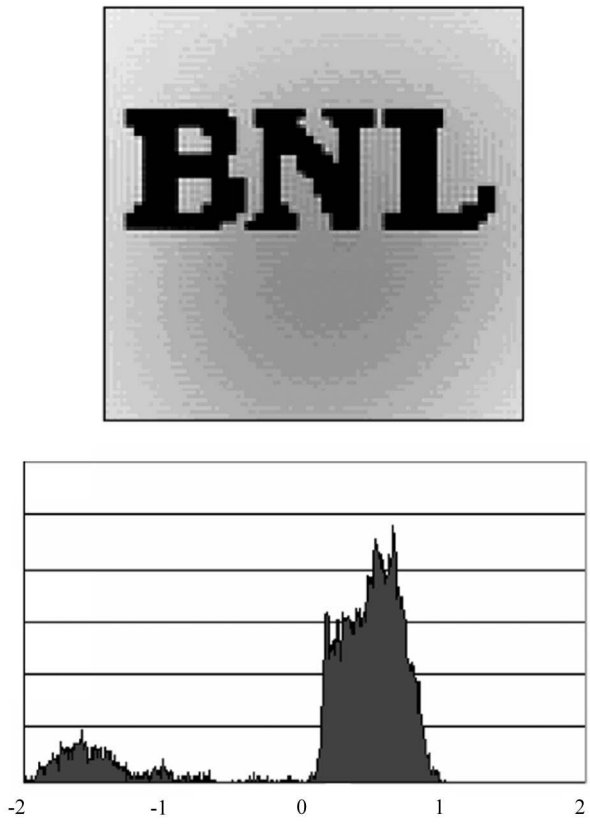

Figure 6
The effect of a 5 × 5 pixel beamstop on the reconstruction. Shown below is the histogram of the reconstructed values. The magnetization for each domain can vary between −1 and +1 after the normalization factors are taken out. Note that the inverse Fourier transform gives values outside this physical range, which are eventually set equal to +1 or −1.

tion in the transmission geometry is best suited for measuring the out-of-plane component of the magnetization density, while linear polarization in the reflection geometry is most sensitive to the in-plane component of the magnetization density. Further, the effect of the beamstop is found to affect the large length scale features of the sample preferentially, and can be overcome by an iterative scheme. Finally, this approach can also explore the interference between the charge scattering and the linear dichroic part of scattering amplitude, which could be used in the imaging of some antiferromagnetic systems.

This research was carried out at the National Synchrotron Light Source, Brookhaven National Laboratory, which is supported by the US Department of Energy, Division of Materials Sciences and Division of Chemical Sciences, under Contract No. DE-AC02-98CH10886.

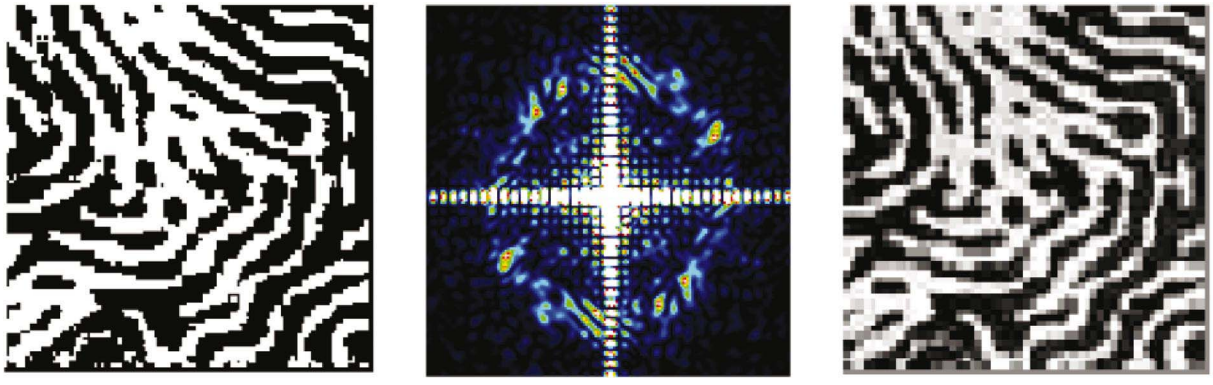

Figure 7
$GdFe_2$ magnetic structure with an average domain size of 110 nm, shown in the first image. The simulated speckle pattern shows the diffraction ring corresponding to the average domain size. The radius of the ring is about 50 pixels. Note that the strong vertical and horizontal features in the diffraction pattern are due to the square shape of the simulated sample. The last image is the reconstructed magnetization density for a 10 × 10 pixel beamstop.

References

Blume, M. (1985). *J. Appl. Phys.* **57**, 3615–3618.

Chen, C. T., Idzerda, Y. U., Lin, H.-J., Smith, N. V., Meigs, G., Chaban, E., Ho, G. H., Pellegrin, E. & Sette, F. (1995). *Phys. Rev. Lett.* **75**, 152–155.

Gibbs, D., Harshman, D. R., Isaacs, E. D., McWhan, D. B., Mills, D. & Vettier, C. (1988). *Phys. Rev. Lett.* **61**, 1241–1244.

Hannon, J. P., Trammell, G. T., Blume, M. & Gibbs, D. (1988). *Phys. Rev. Lett.* **61**, 1245–1248.

Hendrickson, W. A. (1991). *Science*, **254**, 51–58.

Karle, J. (1994). *Resonant Anomalous X-ray Scattering*, pp. 145–158. Amsterdam: Elsevier Science.

Miao, J., Charalambous, P., Kirz, J. & Sayre, D. (1999). *Nature (London)*, **400**, 342–344.

Peters, J. F., de Vries, M. A., Miguel, J., Toulemonde, O. & Goedkoop, J. B. (2000). *ESRF Newslett.* **34**, 15–16.

Sayre, D. (1952). *Acta Cryst.* **5**, 843.

Sayre, D. (1980). *Imaging Processes and Coherence in Physics*, edited by M. Schlenker, M. Fink, J. P. Goedgebuer, C. Malgrange, J. Ch. Viénot & R. H. Wade, pp. 229–235. Berlin: Springer.

Received 24 September 2001 • Accepted 21 January 2002